

QNNet10: A Quantum Neural Network Transfer-Learning Model for Forecasting Problems with Continuous and Discrete Variables

Ismael Abdulrahman, ismael.abdulrahman@epu.edu.iq

Department of Technical Information Systems Engineering, Erbil Technical Engineering College, Erbil Polytechnic University, Erbil 44001, Kurdistan region–Iraq.

Abstract— This study introduces a continuous-variable quantum neural network (CV-QNN) model designed as a transfer-learning approach for forecasting problems. The proposed quantum technique features a simple structure with only eight trainable parameters, a single quantum layer with two wires to create entanglement, and ten quantum gates—hence the name QNNet10—effectively mimicking the functionality of classical neural networks. A noticeable aspect is that the quantum network is trained with random initialization achieving high accuracy and following a single iteration. This pretrained model is innovative as it requires no training or parameter tuning when applied to new datasets, allowing for parameter freezing while enabling the addition of a final layer for fine-tuning. Additionally, an equivalent discrete-variable quantum neural network (DV-QNN) is presented, structured similarly to the CV model. However, the analysis shows that the two-wire DV model does not significantly enhance performance. Consequently, a four-wire DV model is proposed, achieving comparable results but necessitating a larger and more complex structure with additional gates. The pretrained model is applied to five forecasting problems of varying sizes, demonstrating its effectiveness.

Index Terms— quantum computing, machine learning, continuous-variable quantum neural network, discrete-variable, sequential data, load forecasting, transfer learning, Kurdistan demand.

1.1 Introduction

Quantum computers in the near term are available as either superconducting quantum computers, which use the discrete variable (qubit-based) model, or photonic quantum computers, which operate on the continuous variable model. Superconducting computers utilize the particle-like properties of nature, employing individual particles such as electrons as information carriers. These particles can exist in two states, up or down, corresponding to “0” and “1”, making the computational states finite in the qubit model. To maintain the stability of these states, extremely low temperatures are required, necessitating that the chips be housed in dilution systems. Each qubit is connected to classical bit hardware via wires, and sophisticated engineering is needed to control the wire temperature to avoid disturbing the qubit states [1-4].

In contrast, photonic quantum computers use bosonic modes (qumodes) as information carriers, which can be generated and sustained at room temperature using linear optical devices. This makes them easily integrable into existing computing systems. The computational state space of the continuous variable (CV) model, which photonic computers are based on, is infinite-dimensional and allows for a broader range of quantum gates compared to the qubit model [2].

Research on implementing machine learning algorithms on quantum computers is ongoing. Quantum machine learning algorithms can be realized using variational quantum circuits with parametrized quantum gates. A quantum circuit consists of quantum gates, and the change in the initial quantum state caused by the circuit represents quantum computation. The results of quantum computing are obtained through measurement and integrated into optimization and parameter updates on classical circuits [5].

Quantum neural networks (QNNs), a subset of quantum machine learning, operate similarly to classical neural networks. In QNNs, the quantum processing unit (QPU) handles the network operations, while optimization takes place on classical processors. Classical neural networks rely on two main components: linear transformations and nonlinear activation functions. In the qubit-based model, all unitary gates are linear, which makes it difficult to directly implement bias addition and nonlinear activation functions. However, in the continuous variable model, the displacement gate can handle bias addition, and the Kerr gate provides the nonlinear activation function. This enables a natural adaptation of the classical neural network architecture into the quantum framework [5].

The concepts, applications, and challenges of quantum neural networks (QNNs) are presented in [6]. The training process for QNNs is covered in [7], while [8] explores their potential capabilities. Deep QNNs are addressed in [9], with [10] focusing on implementations specifically using superconducting processors. Quantum optimal neural networks are detailed in [11], and quantum convolutional neural networks (CNNs) are explored in [12]. Multi-qubit QNNs are examined in [13]. A concise review of QNN methods and applications is provided in [14], and a scalable, noise-resilient QNN for noisy intermediate-scale quantum (NISQ) computers is presented in

[15]. Additionally, the optimization of QNNs is discussed in [16], a co-design framework for QNNs is outlined in [17], and quantum embedding methods with transformer QNNs for strongly correlated materials are highlighted in [18].

The highlighted studies primarily focus on quantum neural networks based on the qubit model, also known as the discrete variable model. In contrast, the literature reveals only a limited number of studies addressing continuous variable quantum photonic computers. In [19], the adaptability of continuous-variable quantum neural networks is demonstrated through experiments with the Strawberry Fields software library, showcasing applications in fraud detection and image generation. The study proposes a method for building neural networks on quantum computers using a variational quantum circuit in the CV architecture, where the sizes of the later layers are progressively reduced. In [20], Physics-Informed Neural Networks (PINNs) are implemented using a continuous variable quantum framework to tackle the one-dimensional Poisson problem. In [21], an efficient cryptography scheme based on a CV quantum neural network (CV-QNN) is designed for key generation, encryption, and decryption processes on the Strawberry Fields platform. This scheme shows promise for practical applications in quantum devices. In [22], four quantum models are proposed for the CV model using a combination of Gaussian gates (displacement, rotation, squeezing, beamsplitter) and non-Gaussian gates such as the Kerr gate. In [23-24], a detailed introduction to photonic quantum computers is provided.

In this study, a novel CV-QNN transfer-learning model is introduced featuring 2 wires and 8 tunable parameters for sequential forecasting problems. Furthermore, two versions of DV-QNN are developed utilizing qubit-based gates with configurations of 2 and 4 wires. The study employs five datasets, and the results are compared with findings from recent studies.

1.2 Continuous-Variable Quantum Neural Networks

The basic unit of information in continuous variable quantum computing is qumode which is denoted as $|\psi\rangle$ and can be expressed using a quantum state basis expansion as follows [20]:

$$|\psi\rangle = \int \psi(x) |x\rangle dx$$

where the states $|x\rangle$ are eigenstates of the \hat{x} quadrature, with the eigenvalue x being real-valued. This approach is different from the qubit-based system, where the qubit $|\phi\rangle$ is defined as a superposition of the states $|0\rangle$ and $|1\rangle$:

$$|\phi\rangle = \phi_0 |0\rangle + \phi_1 |1\rangle$$

Unlike qubit-based quantum computing, where the coefficients are discrete, the CV model operates on a continuum of

coefficients (continuous eigenvalue spectrum). This distinction underpins the name of this approach. The position (\hat{x}) and momentum (\hat{p}) operators, which define phase space, are examples of continuous quantum operators and play a key role in CV quantum computing. The position operator is defined as:

$$\hat{x} = \int_{-\infty}^{\infty} x |x\rangle \langle x| dx$$

where the vectors $|x\rangle$ are orthogonal. Similarly, the momentum operator is defined as:

$$\hat{p} = \int_{-\infty}^{\infty} p |p\rangle \langle p| dp$$

where $|p\rangle$ are also orthogonal vectors. A qumode is related to a pair of position and momentum operators, (\hat{x}, \hat{p}) , which do not commute, resulting in the Heisenberg uncertainty principle for simultaneous measurements of \hat{x} and \hat{p} . Similar to qubit-based quantum computing, CV quantum computation can also be described using fundamental gates that can be implemented through optical devices. CV quantum programming involves sequences of these gates operating on qumodes. Four fundamental Gaussian gates are known for constructing CV quantum neural networks:

1. **Displacement Gate $D(\alpha)$** : this gate shifts the phase space by a complex number α .

$$D(\alpha): \begin{bmatrix} x \\ p \end{bmatrix} \rightarrow \begin{bmatrix} x + \Re(\alpha) \\ p + \Im(\alpha) \end{bmatrix}$$

2. **Rotation Gate $R(\phi)$** : this operation rotates the phase space by an angle ϕ .

$$R(\phi): \begin{bmatrix} x \\ p \end{bmatrix} \rightarrow \begin{bmatrix} \cos\phi & \sin\phi \\ -\sin\phi & \cos\phi \end{bmatrix} \begin{bmatrix} x \\ p \end{bmatrix}$$

3. **Squeezing Gate $S(r)$** : this gate scales the phase space with a factor r .

$$S(r): \begin{bmatrix} x \\ p \end{bmatrix} \rightarrow \begin{bmatrix} e^{-r} & 0 \\ 0 & e^{-r} \end{bmatrix} \begin{bmatrix} x \\ p \end{bmatrix}$$

4. **Beam-Splitter Gate $BS(\theta)$** : this operation acts as a rotation between two qumodes.

$$BS(\theta): \begin{bmatrix} x_1 \\ x_2 \\ p_1 \\ p_2 \end{bmatrix} \rightarrow \begin{bmatrix} \cos\theta & -\sin\theta & 0 & 0 \\ \sin\theta & \cos\theta & 0 & 0 \\ 0 & 0 & \cos\theta & -\sin\theta \\ 0 & 0 & \sin\theta & \cos\theta \end{bmatrix} \begin{bmatrix} x_1 \\ x_2 \\ p_1 \\ p_2 \end{bmatrix}$$

The first three gates are classified as Gaussian gates which are notable for their ability to preserve the Gaussian nature of quantum states. When applied to a Gaussian state, the output remains a Gaussian state. A key gate derived from other components is the *interferometer*, which can be represented as a combination of beam-splitter and rotation gates. When applied to a single qumode, the interferometer simplifies to a rotation gate. By integrating these Gaussian gates, we can establish an affine transformation, which plays a crucial role in the formulation of neural network computations. In addition, non-Gaussian gates, such as the Kerr or cubic gates, introduce non-linearities analogous to activation functions in classical

neural networks. The Kerr gate, denoted as $K(\kappa)$, plays a significant role due to its availability in quantum simulators.

At the core of quantum computing operations is measurement. In this work, the expected value of the quadrature operator \hat{x} is evaluated after the quantum computations: $\langle \psi_x | \hat{x} | \psi_x \rangle$. A promising approach for implementing CV quantum gates is through photonic technology. An example of such a quantum photonic computer is Xanadu's Borealis quantum computer, which is designed specifically to address Gaussian Boson Sampling (GBS) problems. The field of developing CV quantum computing systems is currently an area of very active research and development, [20, 25-26]. With an understanding of CV quantum gates, their parameters, and the expected value of the quadrature operator, we can proceed to develop a quantum neural network, building upon the foundational work of [20]. The core element of a quantum neural network is the quantum neural network unit, often referred to as a quantum network layer in existing literature, which functions similarly to a classical neural network unit. Figure 1 illustrates the essential components of a quantum neural unit.

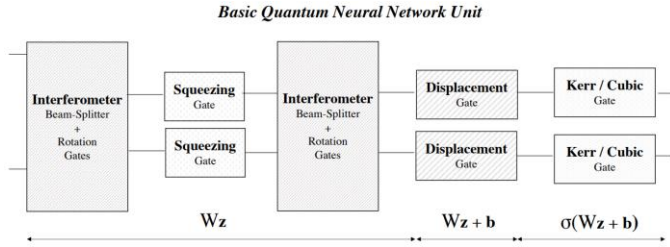


Fig. 1 Components of a quantum neural unit [20]

The first three components consist of a sequence of operations: a first interferometer, a squeezing gate, and a second interferometer. These operations result in an outcome that is comparable to multiplying the phase space vector by the neural network weights W (which correspond to the parameters of the interferometers and squeezing gates). As in classical neural networks, a displacement gate simulates the addition of a bias b . Finally, a Kerr gate (or cubic gate) introduces a non-linearity, analogous to the activation function σ in classical neural networks:

$$|x\rangle \rightarrow |\sigma(Wx + b)\rangle$$

A quantum neural network can be constructed by stacking multiple quantum neural units in a sequential manner. It's crucial to recognize that for each qumode, every gate can be parameterized by seven variables ($\alpha, \phi, r, \theta, \text{ and } \kappa$), which can either be real values ($\phi, r, \theta, \text{ and } \kappa$) or complex numbers (α, r). The complex parameters can be expressed as two real numbers using Cartesian coordinates (real and imaginary parts) or polar coordinates (amplitude and phase). The quantum circuit parameters can be categorized into passive and active parameters: the beam splitter angles and gate phases are passive

parameters, while the displacement, squeezing, and Kerr magnitude are considered active parameters. The training process for quantum neural networks focuses on optimizing the parameter values ($\alpha, \phi, r, \theta, \text{ and } \kappa$) across different qumodes and quantum neural units to minimize the cost function [20]. The number of parameters that these gates can handle for m-qumode circuits is $8m - 2$, as illustrated [5].

The proposed DV-QNN layer architecture

A continuous-variable quantum neural network can be built using a single wire, but such a structure cannot generate entanglement, a core component of any quantum computing system (see [27] for instance). Thus, a two-wire QNN is generally more robust and efficient. However, the network shown in Fig. 1 is relatively complex and requires more trainable parameters with identical gates per wire. Here, the aim is to explore a simpler network that achieves entanglement using basic gates of a CV photonic quantum computer, such as beam splitters, rotations, displacements, squeezers, and nonlinear gates like the Kerr gate. One approach to simplify the network is to "sandwich" squeezing gates between rotation gates, alternating each cycle between a positive and negative direction. The Grover diffusion operator also uses such sandwiching, though here we still require rotation gates to allow the optimizer to find the optimal rotation angles. Therefore, two rotation gates are implemented: one with a fixed quarter-cycle angle and another as an adjustable parameter for optimization. Applying this setup to both wires would increase complexity. Instead, the proposed approach applies the rotation-squeezing sandwiching only on the first wire, while the second wire uses a displacement gate with fixed parameters, such as unity and a quarter-cycle turn. Both wires are connected by two gates that enable entanglement, allowing information sharing across the wires. These gates are the beam splitter and the Cross-Kerr gate. The complete proposed QNN structure will be shown section 1.4 –Fig. 2. Note that the diagram was created using Python, with the parameters shown representing optimized values determined by the optimizer for the problem under study. The entire diagram represents a single-layer QNN. While it is possible to stack multiple such layers for a deeper network, this requires high computational resources. Therefore, the proposed QNN will use only two-wire single layer. For this model, the layer function uses only eight trainable parameters per layer.

1.3 Datasets Descriptions

To verify the effectiveness of the proposed QNN in solving sequential and forecasting problems, the load forecasting dataset for the Kurdistan regional power system is used, as collected by the study [28]. This dataset spans six years (2015–2020), with five years allocated for training and the final year reserved for testing. Additionally, four publicly-available

forecasting datasets from Kaggle are employed in this study including Hourly Electricity Consumption and Production containing 46,011 samples [29], Hourly Energy Consumption by American Electric Power (AEP) containing 121,273 samples [30], Traffic Vehicle Prediction at four traffic junctions containing 48,120 samples [31], and Weather Prediction containing 96,453 samples [32].

1.4 Results of the Proposed CV QNN Model

1.4.1 Dataset 1: Load Forecasting for Kurdistan Demand

In the first dataset, the original study evaluates various scenarios, using either a single feature (load demand in MW) or two features (load demand and weather), both implemented with the proposed network. The experiment runs on a standard computer with 16 GB RAM, a 2.4 GHz processor, and no GPU. For quantum simulations, this study uses PennyLane by Xanadu—an open-source Python-based library supporting both discrete and continuous-variable quantum computations. The network architecture for this dataset is shown in Fig. 2, with initial values randomly set using a Python seed of zero and a learning rate of 0.002 and cut-off dimension of 12 Fock states. The model structure and final parameter values are shown in Fig. 2.

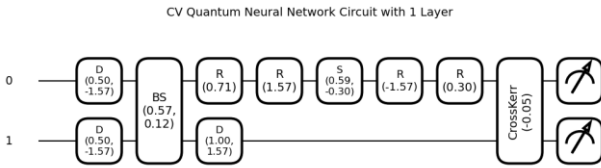


Fig. 2 The proposed CV-QNN architecture with its optimized parameters with demand feature encoded on wire 0

The model is highly nonlinear, creating entanglement across wires, along with a symmetric pattern in the gate configuration and a layered 'sandwiching' of gates. Notably, following the first iteration (*iter 0*), the model achieved a loss of 0.0020201 and root mean squared error of 84.4279 MW—approximately a 3% error relative to a maximum demand of around 2750 MW. During the training, the parameters are slightly altered compared to the initial parameters, which are sufficient to effectively capture the underlying patterns in the training data. In comparing this result with the classical OTSAF model from [28], the proposed model achieved nearly identical accuracy (3.08%) after only one iteration, using a simpler network architecture with only eight tunable parameters. In contrast, the OTSAF network is significantly more complex, featuring several LSTM layers with 128 hidden units each (a unit has three components including reset, update and forget gates), and requires a maximum of 100 training epochs to reach a similar performance level. Moreover, the classical model in [28] struggles with making accurate predictions for closed-loop scenarios. On the other hand, the proposed learning network is

fully quantum, without any classical layers—an advanced approach representing state-of-the-art in quantum machine learning. This fully quantum structure highlights the model’s potential within an emerging field, where quantum machine learning is still in its infancy. Achieving such accuracy with minimal training and no classical components demonstrates the power and promise of quantum architectures, setting a foundation for further advancements in sequential forecasting tasks.

Figure 3a compares the predicted and actual test data after the first iteration, revealing a strong matching between the two. Figure 3b illustrates these predictions across the entire dataset, where the first five years are used for training and the sixth year for testing. In this plot, green represents the predicted values, while red/orange indicates the actual test data. Figure 3c shows the loss per iteration over ten iterations, and Figure 3d displays the sample-wise error in the first iteration.

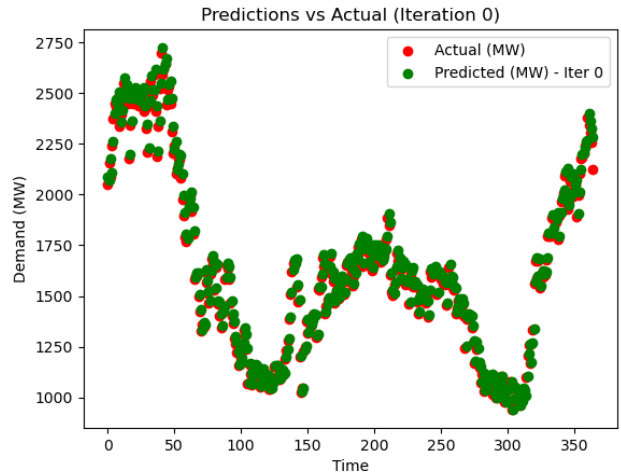


Fig. 3a Actual demand vs prediction for the test samples after only 1 iteration

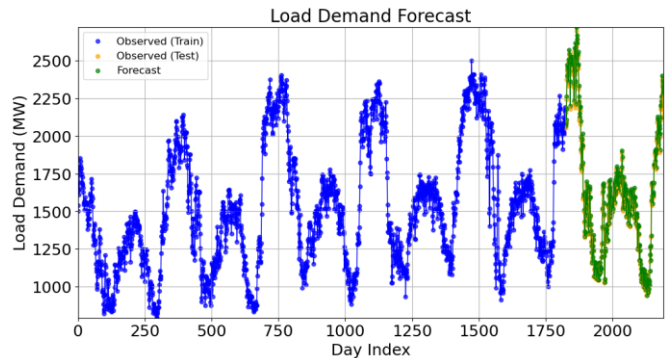


Fig. 3b Training data (blue), test (orange), prediction (green)

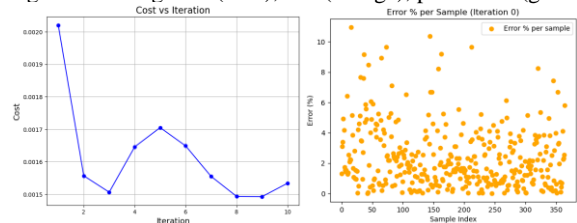


Fig. 3c (left) loss vs iteration and Fig. 3d (right) Error in % between actual and prediction for the test samples

The presented result considers the case where only load demand is to be forecasted. Next, the model is tested with a multi-feature input, incorporating both load demand and weather data (temperature in this study). Each feature is encoded onto a different wire in the quantum circuit: load demand feature is encoded on wire 0 while temperature feature is encoded on wire 1. The model is retrained using the same proposed QNN architecture, with parameters optimized and displayed in Fig. 4a. Notably, after ten iterations, the model achieved a cost of 0.0014932, showing gradual improvement and slightly higher accuracy compared to the single-feature scenario. The predicted vs. actual test data for this multi-feature case is illustrated in Fig. 4b which shows slightly higher accuracy compared to the case with one feature. Notably, almost half of the parameters in the proposed model remain constant, such as those associated with rotations or quarter-cycle displacements, which effectively reduce the training time and the number of parameters needing optimization. This parameter efficiency allows the model to achieve accurate predictions with fewer iterations, conserving computational resources while maintaining performance.

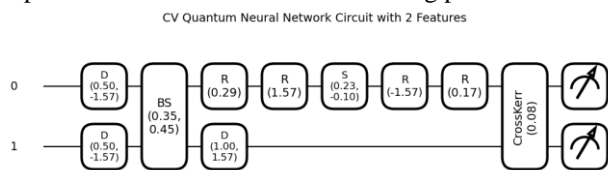


Fig. 4a The proposed CV-QNN architecture for two features: demand and temperature, each is encoded on one wire, and the parameters are re-optimized

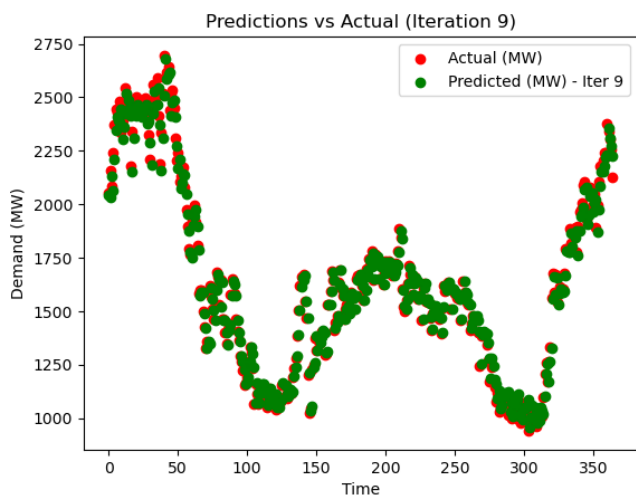


Fig. 4b Actual demand vs prediction for the test samples considering two features: demand and temperature requiring 10 iterations

Another case study is conducted using two input features: the actual demand and its derivative encoded on the two wires individually. The resulting cost of 0.0014827 is comparable to that of the case with demand and temperature. The CV-QNN structure and the predicted vs. actual test data for this case are shown in Figs. 5a and 5b. Notably, the tunable parameters in both multi-feature scenarios have similar values with slightly

alteration, highlighting consistency across double-input feature cases.

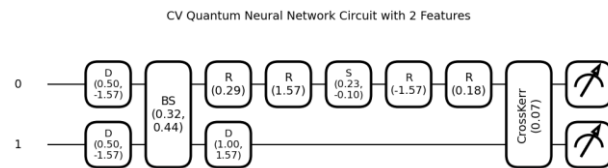


Fig. 5a The proposed CV-QNN architecture for two features: demand and its derivative, each is encoded on one wire and the parameters are re-optimized

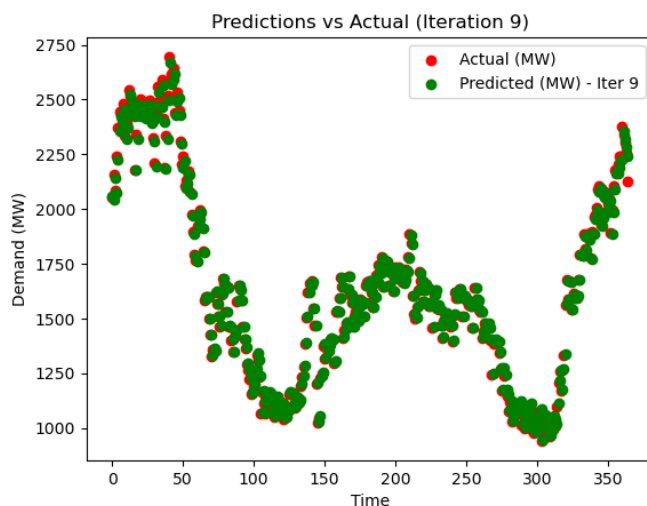


Fig. 5b Actual demand vs prediction for the test samples considering two features: demand and its derivative requiring 10 iterations

The final case study examines Kurdistan's test data, where predictions are made over a multi-step horizon rather than a single-step ahead, as in previous cases. Here, predictions extend one full year forward using the proposed model with the same set of trained parameters. The results, illustrated in Fig. 6, feature a blue scatter plot that represents test data from the last year of the collected dataset, alongside the model's predictions for this unseen test data. The model then projects an additional 365 days forward, effectively capturing and following the dataset's seasonal patterns. The predicted trend retains the characteristic "W" shape driven by the region's four-season cycle.

Unlike the method in [28], which focuses only on test data prediction, this model projects a full year beyond the test range. The proposed method achieves a mean absolute error of 6.3% (171 MW out of 2696 MW), a significant improvement over the 7.99% error reported in [28] using a deep learning approach which is applied only on the test dataset. This outcome underscores the efficiency of this straightforward one-layer model, which, even with a single iteration, outperforms more complex architectures like LSTM and GRU in accurately capturing the dataset's patterns. It's worth noting that the approach where the predicted output at one time step is fed back

as input to predict the following time step is known as *closed-loop* prediction or *feedback* prediction. In this approach, the output forecasted at time step i serves as the input for predicting the subsequent time step $i + 1$. This method allows the model to iteratively build multi-step forecasts by utilizing each predicted value as a stepping stone for the next, effectively creating a self-sustaining prediction sequence.

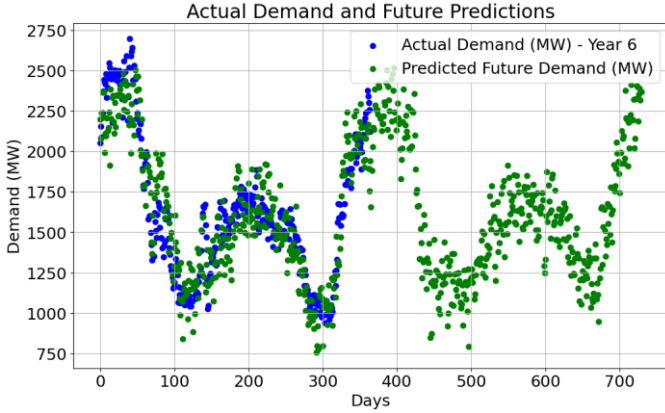


Fig. 6 Multiple time-step ahead forecasting for the following two years

1.4.2 Dataset 2 (Hourly Forecasting Dataset)

To further assess the performance of the proposed model across different datasets, an additional dataset is used featuring hourly electricity consumption and production, sourced from Kaggle [29]. This dataset contains 46,011 samples, which is split into 80% for training and 20% for testing. The same model structure and quantum gates used in Section 1.4.1 is employed for this problem and only the parameters are re-optimized during the training process as illustrated in Fig. 7a. Notably, the parameters remained unchanged, with only a negligible 1% difference in the beam-splitter parameters. Specifically, the first parameter of the BS gate decreased slightly from 0.57 to 0.56, while the second increased from 0.12 to 0.13. For comparison reasons, the pretrained model in Sec. 1.4.1 is loaded and used to predict the energy consumption, yielding the results compared to those obtained by optimizing the parameters through training. This indicates that the model can be applied to new problems and it functions effectively as a transfer learning model. For this problem, the model achieved high performance with a cost of 0.0033. The predictions for the entire test dataset are shown in Fig. 7b, with a zoomed-in view in Fig. 7c, while the sample percentage error is presented in Fig. 7d.

CV Quantum Neural Network Circuit with 1 Layer

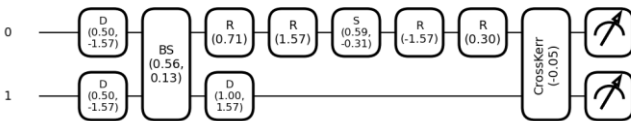


Fig. 7a The proposed CV-QNN architecture for Dataset 2

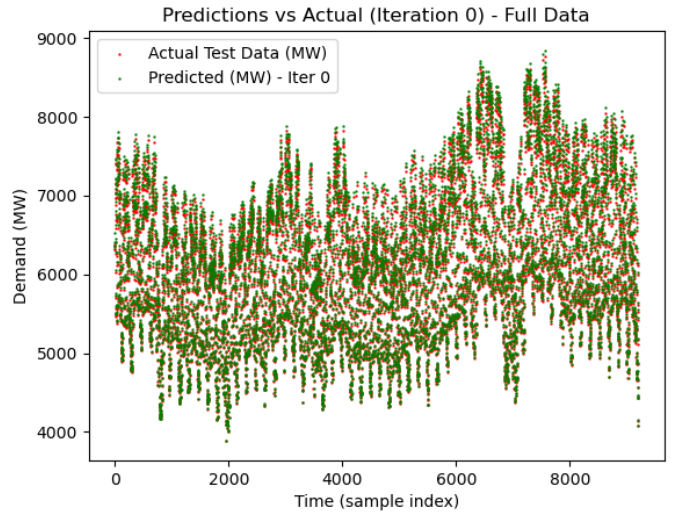


Fig. 7b Actual vs prediction for the entire test split of Dataset 2

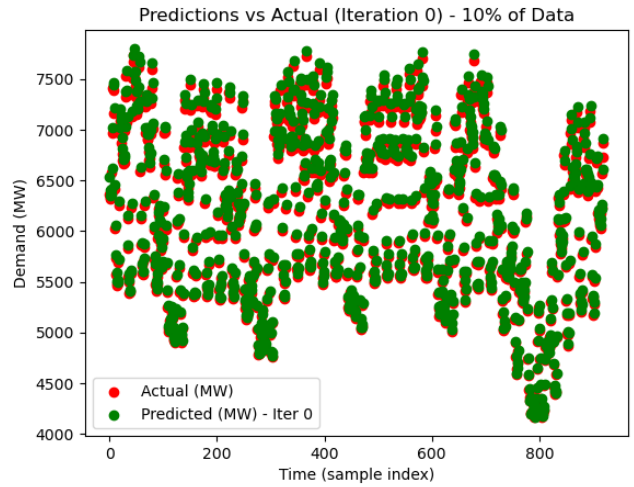


Fig. 7c Zoomed-in view of Fig. 7a: 10% Magnification

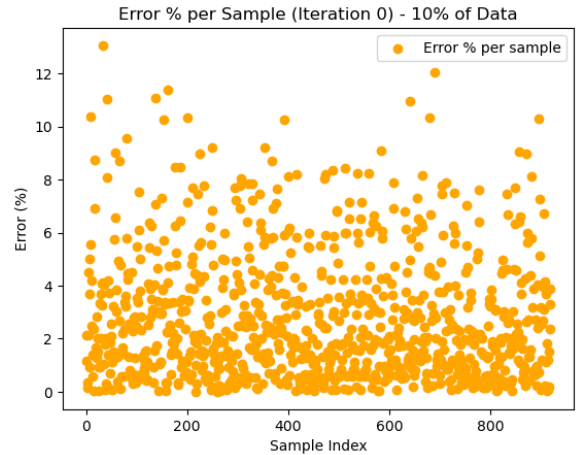


Fig. 7d Sample error in % for the zoomed-in view of Dataset 2

1.4.3 Dataset 3 (Hourly Energy Consumption)

The third dataset, also publicly available on Kaggle, contains a larger dataset of 121,273 samples representing hourly energy consumption provided by the American Energy Power (AEP) [30]. This dataset was first trained and tested using the same proposed model in Sec. 1.4.2. The model achieved an error of

730 MW compared to a maximum demand of 25,695 MW, resulting in an overall percentage error of 2.8%. Notably, with only one iteration and parameters almost identical to those used for Datasets 1 and 2, the model attained high accuracy. This demonstrates the model's effectiveness in predicting similar types of forecasting problems. Since the parameters optimized during training on Datasets 2 and 3 show almost no variation—differing only by 1% in the beam splitter—we can conclude that the proposed model effectively operates as a transfer learning network, with parameters that are well-suited for any similar forecasting dataset. To confirm this, the model trained on Dataset 2 was saved and then reloaded with its optimized parameters for use on Dataset 3. The results obtained were identical to those achieved from training directly on Dataset 3, but this time achieved without any additional training, simply by using the pretrained model presented in Sec. 1.4.2. The predictions are plotted in Figs. 8a using the entire test dataset.

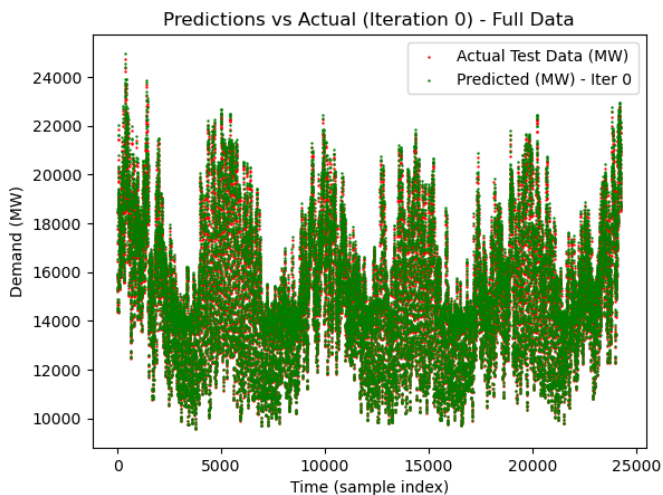


Fig. 8a Actual vs prediction for the entire test part of Dataset 3 using the transfer-learning model in Sec. 1.4.2

For the same problem, multi-time-step close-loop forecasting is conducted using the pretrained model, predicting 365×24 samples. The predictions, shown in green in Fig. 8b appended to the test data in blue, show that the model effectively captures the patterns in the historical data.

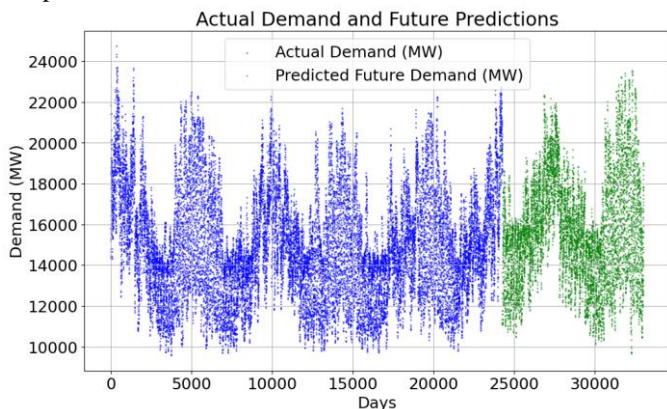


Fig. 8b Multiple time-step ahead forecasting for the following year using the transfer-learning model in Sec. 1.4.2

1.4.4 Dataset 4 (Traffic Vehicle Prediction)

In this section, a different forecasting problem is considered: Traffic Vehicle Prediction [31]. This dataset contains a total of 48,120 samples across four junctions. For this task, predictions are made for vehicles at Junction 1, with 14,591 samples in total, split into 11,672 for training and 2,919 for testing. The predictions are plotted in Fig. 9a using the entire test dataset. For this problem, multi-time-step closed-loop forecasting is also performed using the pretrained model, predicting samples for around next two years. As shown in Fig. 8b, future predictions (in green) are appended to the test data (in blue), demonstrating with the other plots that the model effectively captures patterns in the historical data.

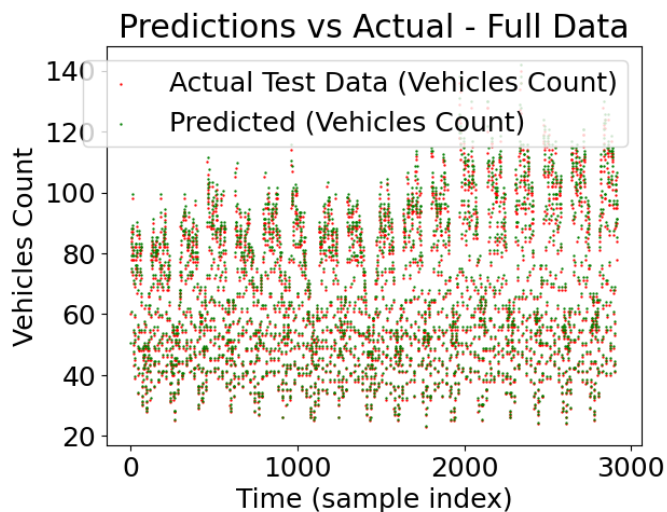


Fig. 9a Actual vs prediction for the entire test part of Dataset 4 using the transfer-learning model in Sec. 1.4.2

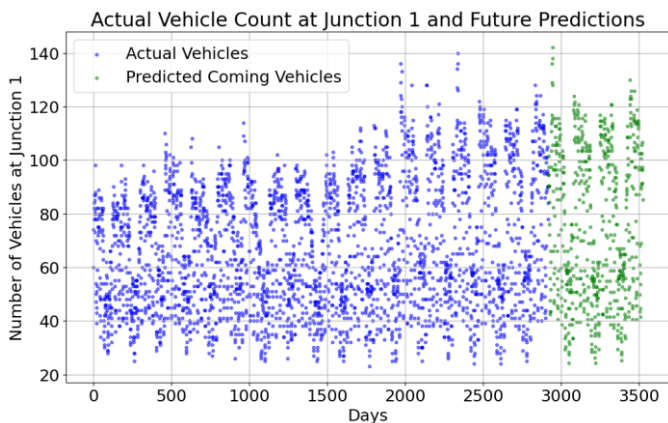


Fig. 9b Multiple time-step ahead forecasting for the following year

1.4.4 Dataset 5 (Weather Prediction)

Lastly, another forecasting problem is examined: Weather Prediction, focusing on the temperature feature, though the model can be applied to other features as well [31]. This dataset contains a total of 96,453 samples, split into 80% for training and 20% for testing. Predictions for the entire dataset are shown in Fig. 10a, while Fig. 10b presents the multi-step forecast. For

this task, both open-loop single-step predictions and closed-loop multi-step forecasting are performed using the pretrained model to predict temperature samples for the entire following year. Although temperature is typically better suited for predicting the next hour or few days, the focus here is on the pretrained model's ability to extract patterns across different types of data. As illustrated in Fig. 10b, predictions (in green) are appended to the test data (in blue), demonstrating that the model effectively captures historical patterns, as confirmed by the other plots.

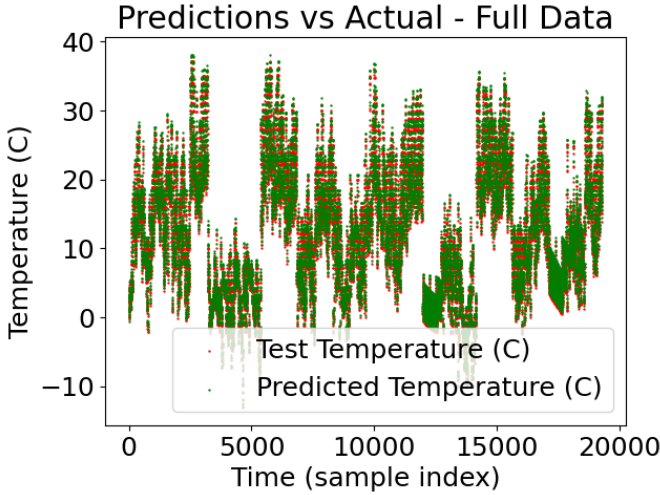


Fig. 10a Actual vs prediction for the entire test part of Dataset 5 using the transfer-learning model in Sec. 1.4.2

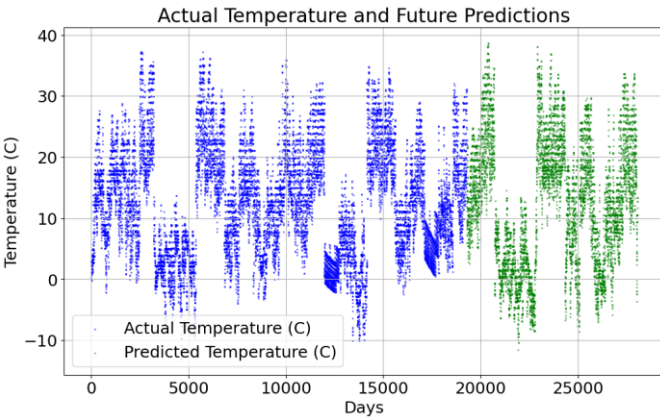


Fig. 10b Multiple time-step ahead forecasting for the following year

1.5 Discrete Qubit-Based Approach

In section 1.2 a simple and effective continuous variable (CV) QNN architecture is proposed for solving sequential machine learning problems, particularly time series forecasting. In this section, an alternative quantum approach using discrete variables (DV) is investigated. The DV model shows promise for addressing the same problem; however, as we will see, it requires a more complex structure, deeper networks, and achieves lower accuracy than the previous proposed CV model. Nonetheless, it is worth discussing here in this paper.

Here, beginning with the DV version of the same model proposed in the CV approach, utilizing popular discrete quantum gates such as RX , RZ , RY , and $CNOT$ gates. Specifically, a two-wire system is employed, as in the CV model, and the Hadamard and $CNOT$ gates are used to create entanglement. In the first wire, an RZ gate is placed between two RY gates each side, creating a "sandwiched" structure. One RY gate is set to a quarter-cycle angle, while the other is optimized to function as a rotation gate, serving as a weight parameter similar to those in classical neural networks. In the second wire, an RX gate is used as a bias parameter, which is also optimized, followed by an additional $CNOT$ gate to create further entanglement, analogous to the Cross-Kerr gate. This approach mirrors the configuration used in the CV model.

The proposed model is applied to forecast load demand in Kurdistan with the same train-test split ratio. The optimized parameters and model structure are shown in Fig. 11a. After one training iteration, the predicted demand and error per sample are displayed in Fig. 11b-c. The model shows promising ability to learn and follow patterns hidden in the data. However, increasing number of iterations or even the depth of circuit or tuning hyperparameters was not found to be particularly helpful. Additional refinements are necessary to enhance its predictive accuracy.

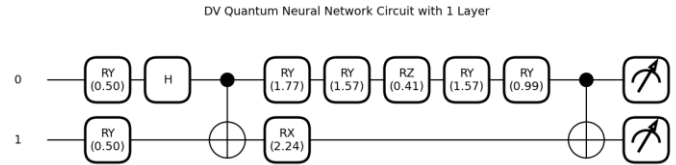


Fig. 11a The proposed qubit-based 2-wire DV QNN model

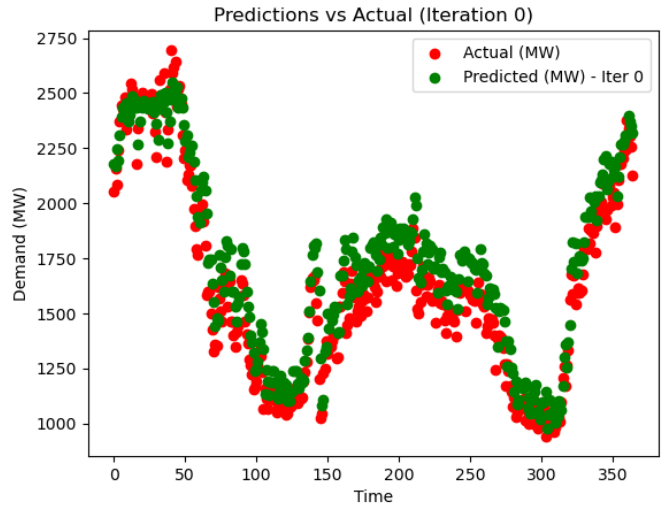


Fig. 11b Actual vs prediction for the test samples after 1 iteration using the 2-wire DV QNN model

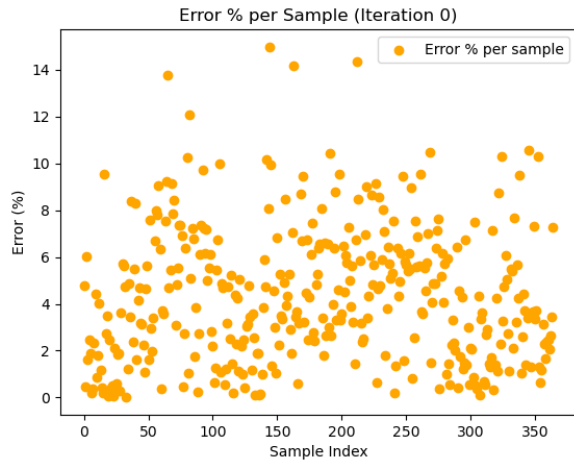


Fig. 11c Sample error in % after 1 iteration for Dataset 1 using the DV QNN model with 2 wires

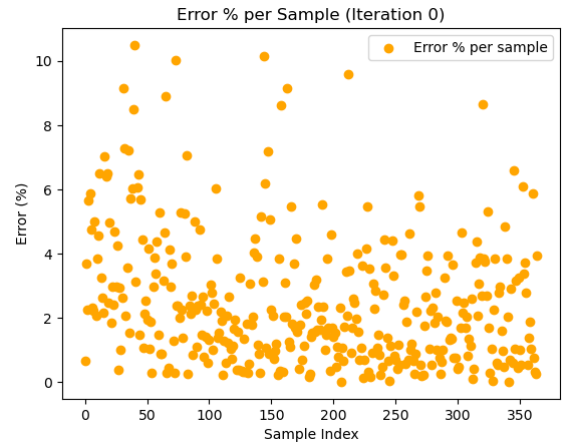


Fig. 12c Sample error in % after 1 iteration for Dataset 1 using the DV QNN model with 4 wires

To enhance its performance, a double two-wire architecture is proposed, introducing additional entanglements across all wires. This configuration doubles the wire count to four, with the third and fourth wires replicating the structure and gates used in the first two wires as shown in Fig. 12a. A total of eight parameters are optimized with a learning rate set at 0.01 and initial values generated randomly, using only one layer. The results and error per sample, as shown in Fig. 12b-c, indicate clear improvement over the single two-wire structure, achieving an error of 86 MW (3.19%). However, this approach requires twice the parameters comparing to the simple two-wire version, additional entanglements, longer training time, with a lower processing speed.

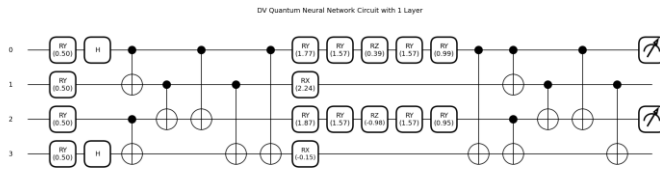


Fig. 12a The proposed qubit-based 4-wire DV QNN Predictions vs Actual (Iteration 0)

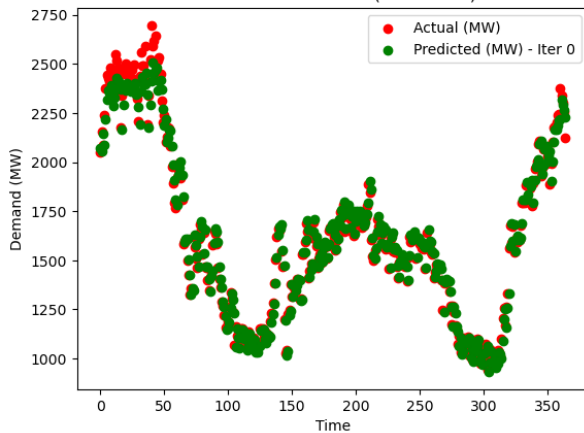


Fig. 12b Actual vs prediction for the test samples after 1 iteration using the 4-wire DV QNN model

1.6 Conclusion

This study presented a novel continuous-variable quantum neural network (CV-QNN) named QNNet10 for sequential forecasting tasks, paving the way for quantum architectures to become a viable approach to traditional deep learning solutions. The proposed CV-QNN model achieves high accuracy with minimal complexity, utilizing only a single layer, two wires, and eight trainable parameters. Applied to load forecasting for the Kurdistan regional power system and 4 additional different datasets, the model demonstrated its capability to capture complex patterns with minimal parameter adjustments and computational resources, achieving accuracies on par with state-of-the-art deep learning models. The study also highlights the robustness of CV-QNN in transfer learning applications, where freezing initial layers while fine-tuning with a final layer facilitates adaptation across datasets. The model's success in multi-step forecasting and multi-feature scenarios further confirms its flexibility and accuracy, meeting a key need in sequential forecasting applications.

Additionally, a discrete-variable quantum neural network (DV-QNN) approach was investigated, proposing two-wire and four-wire configurations with discrete quantum gates. The two-wire DV-QNN, while promising, requires a more complex structure and yields lower accuracy compared to the CV-QNN. To improve performance, a four-wire configuration is proposed, enhancing entanglement. However, this model necessitates additional parameters and longer training times, indicating a trade-off between accuracy and computational efficiency. Overall, the findings highlight the strengths of the CV-QNN model while illustrating the potential and challenges of the DV-QNN in sequential machine learning tasks.

Demonstrating Video

<https://drive.google.com/file/d/1sXGvS1FSXQoysJYTcPIVnqOrl-Wqbi3k/view?usp=sharing>

Funding

No financial support is provided for this work.

Conflict of Interest

The authors declare that there is no conflict of interest associated with this work.

Data and Code Availability

Datasets 2 and 3 are publicly accessible [29]–[30]; however, Dataset 1 cannot be shared publicly due to certain restrictions by the provider. The corresponding Python codes developed specifically for this paper can be shared upon reasonable request.

Biography

Ismael Abdulrahman received his PhD in Electrical and Computer Engineering from Tennessee Technological University, USA, in 2019. Currently, he serves as an assistant professor at Erbil Polytechnic University, where he instructs graduate and undergraduate courses including quantum computing, advanced deep learning, advanced mathematics, and electrical and electronic courses. His academic passions include quantum computing, deep learning, optimization, and mathematical modeling.



References

- 1 Nielsen, Michael A., and Isaac L. Chuang. *Quantum Computation and Quantum Information*. Cambridge University Press, 2010.
- 2 Choe, Sophie. “Quantum Computing Overview: Discrete vs. Continuous Variable Models Superconducting vs. Linear Optics,” 2022. arXiv:2206.07246v1.
- 3 Easttom, Chuck. *Hardware for Quantum Computing*. Springer, 2024.
- 4 *Quantum Computing: Progress and Prospects*. Consensus Study Report. The National Academic Press, 2019.
- 5 Choe, Sophie, and Marek Perkowski. “Continuous Variable Quantum MNIST Classifiers.” *Journal of Quantum Information Science* 12 (2022): 37-51.
- 6 Kwak, Y., and J. Yun et al. “Quantum Neural Networks: Concepts, Applications, and Challenges.” arXiv:2108.01468v1, 2021.
- 7 Beer, K., D. Bondarenko et al. “Training Deep Quantum Neural Networks.” *Nature Communications*, 2020.
- 8 Abbas, A., and D. Sutter. “The Power of Quantum Neural Networks.” *Nature Computational Science*, 2021.
- 9 Zhao, C., and X. Gao. “QDNN: Deep Neural Networks with Quantum Layers.” *Quantum Machine Intelligence*, 2021.
- 10 Pan, X., Z. Lu et al. “Deep Quantum Neural Networks on a Superconducting Processor.” *Nature Communications*, 2022.
- 11 Steinbrecher, G., and J. Olson. “Quantum Optical Neural Networks.” *Quantum Information*, 2019.
- 12 Cong, I., S. Choi et al. “Quantum Convolutional Neural Networks.” *Nature Physics*, 2019.
- 13 Ban, Y., E. Torrontegui et al. “Quantum Neural Networks with Multi Qubit Potentials.” *Scientific Reports*, 2023.
- 14 Jia, Z., B. Yi, et al. “Quantum Neural Network States: A Brief Review of Methods and Applications.” *Advanced Quantum Technologies*, 2019.
- 15 Alam, A., and S. Ghosh. “QNet: A Scalable and Noise-Resilient Quantum Neural Network Architecture for Noisy Intermediate-Scale Quantum Computers.” *Frontiers in Physics*, 2022.
- 16 Chen, A., and M. Heyl. “Empowering Deep Neural Quantum States Through Efficient Optimization.” *Nature Physics*, 2023.
- 17 Jiang, W., J. Xiong et al. “A Co-Design Framework of Neural Networks and Quantum Circuits Towards Quantum Advantage.” *Nature Communications*, 2021.
- 18 Ma, H., and H. Shang et al. “Quantum Embedding Method with Transformer Neural Network Quantum States for Strongly Correlated Materials.” *NPJ Computational Materials*, 2024.
- 19 Killoran, N., and T. Bromley. “Continuous-Variable Quantum Neural Networks.” *Physical Review Research*, 2019.
- 20 Markidis, Stefano. “On Physics-Informed Neural Networks for Quantum Computers.” arXiv:2209.14754v2, 2022.
- 21 Shi, J., S. Chen et al. “An Approach to Cryptography Based on Continuous-Variable Quantum Neural Network.” *Scientific Reports*, 2020.
- 22 *Quantum Neural Network — Strawberry Fields*. Retrieved 2024.
- 23 Ballon, Alvaro. “Photonic Quantum Computers.” PennyLane, 2024. *Photonic Quantum Computers | PennyLane Demos*.
- 24 Killoran, N., J. Izaac et al. “Strawberry Fields: A Software Platform for Photonic Quantum Computing.” Xanadu, arXiv:1804.03159v2.
- 25 Madsen, L. S., Laudenbach, F., Askarani, M. F., Rortais, F., Vincent, T., Bulmer, J. F., Miatto, F. M., Neuhaus, L., Helt, L. G., Collins, M. J., et al. “Quantum Computational Advantage with a Programmable Photonic Processor.” *Nature* 606, no. 7912 (2022): 75–81.
- 26 Fukui, K., and Takeda, S. “Building a Large-Scale Quantum Computer with Continuous-Variable Optical Technologies.” *Journal of Physics B: Atomic, Molecular and Optical Physics* 55, no. 1 (2022): 012001.
- 27 Xanadu. “Quantum Neural Network.” Retrieved on 30/10/2024. *Quantum Neural Network — Strawberry Fields*.
- 28 Hamad, Z., and I. Abdulrahman. “Deep Learning-Based Load Forecasting Considering Data Reshaping Using MATLAB/Simulink.” Volume 13 (2022): 853–869.
- 29 Kaggle’s Hourly Electricity Consumption and Production, URL: <https://www.kaggle.com/datasets/stefancomanita/hourly-electricity-consumption-and-production>
- 30 American Energy Power (AEP) – Hourly Energy Consumption The dataset "Hourly Energy Consumption" is available at: <https://www.kaggle.com/datasets/robikscube/hourly-energy-consumption>

- 31 Kaggle's Traffic Prediction Dataset (Four Junctions),
URL: <https://www.kaggle.com/datasets/fedesoriano/traffic-prediction-dataset>
- 32 Kaggle's Weather Prediction Dataset,
URL: <https://www.kaggle.com/datasets/muthuj7/weather-dataset>